Brain Struct Funct (2012) 217:19–36
DOI 10.1007/s00429-011-0329-6

ORIGINAL ARTICLE

Distribution of SMI-32-immunoreactive neurons in the central auditory system of the rat

Ladislav Ouda · Rastislav Druga · Josef Syka

Received: 12 February 2011 / Accepted: 11 May 2011 / Published online: 9 June 2011

Abstract SMI-32 antibody recognizes a non-phosphorylated epitope of neurofilament proteins, which are thought to be necessary for the maintenance of large neurons with highly myelinated processes. We investigated the distribution and quantity of SMI-32-immunoreactive(-ir) neurons in individual parts of the rat auditory system. SMI-32-ir neurons were present in all auditory structures; however, in most regions they constituted only a minority of all neurons (10–30%). In the cochlear nuclei, a higher occurrence of SMI-32-ir neurons was found in the ventral cochlear nucleus. Within the superior olivary complex, SMI-32-ir cells were particularly abundant in the medial nucleus of the trapezoid body (MNTB), the only auditory region where SMI-32-ir neurons constituted an absolute majority of all neurons. In the inferior colliculus, a region with the highest total number of neurons among the rat auditory subcortical structures, the percentage of SMI-32-ir cells was, in contrast to the MNTB, very low. In the medial geniculate body, SMI-32-ir neurons were prevalent in the ventral division. At the cortical level, SMI-32-ir neurons were found mainly in layers III, V and VI. Within the auditory cortex, it was possible to distinguish the Te1, Te2 and Te3 areas on the basis of the variable numerical density and volumes of SMI-32-ir neurons, especially when the pyramidal cells of layer V were taken into account. SMI-32-ir neurons apparently form a representative subpopulation of neurons in all parts of the rat central auditory system and may belong to both the inhibitory and excitatory systems, depending on the particular brain region.

Keywords SMI-32 · Superior olivary complex · Inferior colliculus · Medial geniculate body · Auditory cortex · Rat

L. Ouda (✉) · J. Syka
Institute of Experimental Medicine, Academy of Sciences of the Czech Republic, Vídeňská 1083, 142 20 Prague, Czech Republic
e-mail: ouda@biomed.cas.cz

R. Druga
Department of Anatomy, 1st and 2nd Medical Faculty, Charles University, Prague, Czech Republic

Introduction

Neurofilament proteins are neuron-specific cytoskeletal intermediate filaments essential for the development and maintenance of neurons and their processes (Hoffman et al. 1987; Lee and Cleveland 1994). Among them, three structurally and genetically related proteins form a so-called triplet, consisting of light, medium and heavy neurofilament subunits (Vickers and Costa 1992). The monoclonal antibody SMI-32 (Sternberg Monoclonals Incorporated, product no. 32), which recognizes the non-phosphorylated epitope of the medium and heavy neurofilament subunits, has been shown to specifically label the dendrites and perikarya of a subset of neocortical pyramidal neurons with subcortical axonal projections (Sternberger and Sternberger 1983; Kirkcaldie et al. 2002; Voelker et al. 2004; Molnár and Cheung 2006). The content of neurofilament triplets in neurons is thought to be associated with the level of myelination and to be related to the fast conduction of axons (Lawson and Waddell 1991; Kirkcaldie et al. 2002). The neurofilaments are thought to be necessary for structural stability and to be involved in nutrition transport in large, fast firing neurons with long processes (Goldstein et al. 1987; Lasek 1988).

The subset of cortical neurons labeled with SMI-32 antibody was found to be preferentially lost in Alzheimer's and Huntington's diseases (Cudkowicz and Kowall 1990; Hof and Morrison 1990). SMI 32 antibody was also shown

to be a sensitive marker for early and chronic lesions in multiple sclerosis, including discontinuous immunostaining of demyelinating axons and, especially, of axon-terminal spheroids, indicative of axonal disintegration in multiple sclerosis (Trapp et al. 1998). In an animal model of multiple sclerosis, SMI-32 immunoreactivity was found to be diminished under demyelinisation processes in marmosets during autoimmune encephalomyelitis (Mancardi et al. 2001). SMI-32 positivity was also substantially decreased in the cat lateral geniculate body under conditions of induced early visual deprivation (Bickford et al. 1998; Duffy and Slusar 2009). These results suggest that SMI-32-immunoreactive(-ir) neurons are highly vulnerable to different pathological processes and, consequently, the deterioration of non-phosphorylated neurofilaments may contribute to the further development of pathological changes. In addition, aged C57 mice were shown to be more prone to the loss of SMI-32 immunoreactivity during induced demyelinisation processes than young animals (Irvine and Blakemore 2006). The neurofilament content is also altered with normal aging, presumably due to rising neurofilament phosphorylation in the senescent brain (Vickers et al. 1992; Veeranna et al. 2009), which may further contribute to greater age-dependent vulnerability.

Recently, growing evidence has shown that differences in the immunohistochemical pattern of SMI-32 expression can be successfully used for the parcellation of cortical areas, the hippocampus and perihippocampal areas in different mammalian species, e.g. in monotremes (Hassiotis et al. 2004), rodents (Budinger et al. 2000; Bajo and Moore 2005; Boire et al. 2005), felines (Van der Gucht et al. 2001; Lee and Winer 2008b, c) as well as in primates (Chaudhuri et al. 1996; Baldauf 2005; Luppino et al. 2005). The data about SMI-32 immunoreactivity in subcortical structures are limited. The distribution of SMI-32-ir neurons was described in the striatopallidal complex of humans and monotremes (Morel et al. 2002; Ashwell 2008). Differences between the magnocellular and parvocellular layers of the lateral geniculate body based on SMI-32 immunoreactivity were reported in primates (Bourne and Rosa 2003; Soares et al. 2008). In the auditory system, SMI-32-ir neurons were found to be present in some nuclei of the human superior olivary complex (Bazwinsky et al. 2003).

The primary aim of this study was to investigate the distribution of SMI-32-immunoreactive neurons within the rat central auditory system and to estimate their numbers in individual regions of the auditory system in comparison with the total number of neurons. Detailed knowledge of the distribution and percentage of SMI-32-ir neurons in particular subcortical and cortical auditory structures is important to both identify this potentially vulnerable neuronal population and also for better understanding of the functional significance of the SMI-32-ir population in particular structures. To accomplish this aim, reliable knowledge of the total number of neurons in particular brain region is necessary. To date, only a very few unbiased assessments have been performed to determine the total number of neurons in the particular nuclei and regions of the rat central auditory system (Kulesza et al. 2002). In the present study, we used unbiased stereological methods to estimate both the number of SMI-32-ir neurons and the total number of neurons in individual nuclei and areas of the auditory pathway. In addition, we also aimed to elucidate whether the parcellation of cortical areas based on the SMI-32 immunoreactivity pattern could be quantified with respect to the number and volumes of SMI-32-ir neurons in particular adjacent areas (auditory and surrounding non-auditory cortical areas).

Materials and methods

Animals

Experiments were performed on young adult (3–6 months old) pigmented rats (strain Long Evans), which were obtained from a local facility and were reared in-house under standard conditions. No signs of middle ear infection were present in any animal during their stay in the animal house. The care and use of animals and all experimental procedures followed the principles of laboratory animal care and were performed in compliance with the guidelines of the Ethical Committee, Institute of Experimental Medicine, Academy of Sciences of the Czech Republic, and the Declaration of Helsinki.

Immunohistochemistry

Rats ($n = 10$) were placed under deep anesthesia (ketamine 50 mg/kg + xylazine 8 mg/kg, i.m.) and then transcardially perfused with saline followed by 4% paraformaldehyde fixative in 0.1 M phosphate buffer (pH 7.4). The brains were removed within 15 min of perfusion, postfixed 1 h at 4°C (same fixative) and then cryoprotected with 30% sucrose in phosphate buffer overnight. Coronal serial sections (40 μm thick) were cut with a freezing microtome.

Free-floating sections were preincubated in a blocking solution (5% low fat milk in PBS, 1 h) and then immersed in PBS containing the mouse monoclonal antibody SMI-32 against non-phosphorylated heavy and medium neurofilament subunits (1:1,000, Covance Research Products, USA) for 18 h (4°C). In the next step, the sections were incubated with a biotinylated goat anti-mouse secondary antibody (1:200, Sigma) for 1 h, and then with avidin–biotin–peroxidase complex (1:100, Vector) for 1 h at room temperature. The reaction was visualized with 0.02% diaminobenzidine

and 0.01% hydrogen peroxide. Finally, the sections were mounted on slides, dehydrated and coverslipped.

Negative control staining to check for false positivity was performed using the same procedure but with the omission of the primary antibody; no immunopositivity was observed in the control sections (1 section per animal, from 4 animals). The positive specifity of the antibody was primarily established based on the data provided by the manufacturer and the report by Kirkcaldie et al. (2002), who demonstrated that SMI-32 labeled essentially all cortical neuronal somata that were immunoreactive with other antibodies to different non-phosphorylated neurofilament subunits and vice versa; i.e., the neurons that were negative with the other antibodies were also negative for SMI-32 labeling.

Simultaneously, each second section from a subgroup of animals ($n = 6$) was used for Nissl staining using a standard protocol (0.2% cresyl violet acetate).

Microscopy, imaging and stereological quantification

SMI-32 immunoreactivity was examined in all sections containing the cochlear nuclei (CN), superior olivary complex (SOC), nuclei of the lemniscus lateralis (LL), inferior colliculus (IC), medial geniculate body (MGB) and auditory cortex (AC). These structures were delineated according to anatomical atlases (Zilles 1985; Paxinos and Watson 1998) and with the help of Nissl-stained sections (topographical borders of the cortical auditory areas and subdivisions of the subcortical auditory regions). In total, sections from ten animals were used for the analysis. The CN, SOC and LL sections were obtained from six animals and the IC, MGB and AC sections from ten animals. In addition, Nissl-stained sections from six animals, comprising all the mentioned auditory structures, were included into the analysis to provide a basis for calculating the total number of neurons in the indicated structures and to estimate the percentage of SMI-32-ir cells from the total number of neurons.

Measurements were performed using bright-field microscopy (Olympus BX-51) coupled with a X–Y–Z motorized stage and connected to a video camera, which transmitted the data to a computer and displayed them on a monitor. Stereo Investigator software (MicroBrightField, Inc.) was used to perform the optical dissector and nucleator protocol (West et al. 1991; Mayhew and Gunderesen 1996; Andersen and Gundersen 1999).

First, we randomly selected a section containing the analyzed auditory structure, outlined the selected area of interest (4× or 10× objective lens) and then uniformly sampled the selected area of interest. The stereological probes were used in conjunction with a 100× objective lens, while the counting frames used to obtain the sampling always had the same size in all examined regions (2,500 μm^2) and were formed by two inclusion lines and two exclusion lines. The frequency of samples depended on the size of the structure (section fraction). While the original thickness of the sections was 40 μm, due to the tissue processing, the average thickness was reduced to approximately 23 μm (for SMI-32) or 20 μm (for Nissl staining). The height of the optical dissector was constant at 10 μm for both stainings and the first and last 5 μm of the section thickness were omitted from the analysis (guard zones).

Each neuron in the counting frame was counted when its nucleus came into maximum focus. Only SMI-32-ir somas that contained a distinct nucleus and cytoplasm were counted and used for the analysis. In Nissl staining, glia cells were omitted from analysis based on limited or non-visible cytoplasm and small dark nuclei. Likewise, small granule cells in the dorsal cochlear nucleus were not counted in Nissl staining due to the difficulty of differentiating them from glia cells.

The neuronal estimate for a given structure (N_{est}) was calculated as N_{est} = number of counted cells × area fraction × section fraction × dissector fraction.

The coefficient of error (CE) is a standard statistical value for a study with stereological tools. The CE is basically defined as the SEM divided by the group mean. The group coefficient of error gives an estimate of the accuracy of the estimate of the mean calculated for each subject group. Estimates of the coefficient of error (CE) were calculated with the Gundersen–Jensen estimator (Gundersen et al. 1999) using a smoothness constant (m) of 1. The estimates of the number of cells in individual cortical layers served as a brief survey with a high coefficient of error; therefore, the results of this survey were not included into Table 1.

In addition, variations in the distribution of SMI-32-ir neurons throughout the coronal sections of the temporal (auditory and non-auditory) cortices were examined by counting the SMI-32-ir cells separately within six strips (each 1 mm wide), superimposed on the cortical coronal sections, with the first strip starting in the fissura rhinalis. Therefore, the strips overlapped the perirhinal, ectorhinal, auditory and partially the parietal cortex as shown in a schematic section through the forebrain (Fig. 1). Further, SMI-32 neuronal volumes were also measured, using the nucleator technique, within the superimposed strips shown in Fig. 1. In contrast to the unbiased counting of neurons, these measurements of neuronal volume could contain a small error. Because the sections were cut coronally (to differentiate the brain regions according to the atlases) the requirement of an isotropic or vertical random orientation of the sections could not be met (Mayhew and Gunderesen 1996). However, the measurement of neuronal volumes served only for auxiliary quantitative analysis to compare

Table 1 Unbiased estimates (N_{est}) of the total number of neurons (Nissl), the number of SMI-32-ir neurons and the percentage of SMI-32-ir neurons in the auditory pathway of the rat

Structure	All neurons	CE	SMI-32-ir neurons	CE	Portion of SMI-32-ir neurons (%)
Cochlear nuclei (CN)					
Anteroventral CN	15,700	0.04	4,970	0.04	32
Posteroventral CN	7,500	0.04	2,240	0.03	30
Dorsal CN	9,900	0.05	1,440	0.05	15
Total number	33,100		8,650		
Superior olivary complex					
Medial nucleus of the trapezoid body	5,400	0.03	3,120	0.03	58
Lateral superior olive	3,900	0.05	740	0.04	19
Medial superior olive	900	0.07	100	0.08	11
Superior paraolivary nucleus	2,000	0.05	490	0.04	25
Lateroventral periolivary nucleus	1,300	0.05	270	0.05	20
Medioventral periolivary nucleus	2,800	0.06	740	0.06	26
Total number	16,300		5,460		
Nuclei of the lateral lemniscus (LL)					
Dorsal LL	2,100	0.06	660	0.07	31
Intermediate LL	3,600	0.05	810	0.06	23
Ventral LL	9,200	0.05	1,890	0.05	21
Total number	14,900		3,360		
Inferior colliculus (IC)					
Dorsal cortex of the IC	43,600	0.04	3,190	0.05	7
External cortex of the IC	80,600	0.04	8,360	0.04	10
Central nucleus of the IC	195,300	0.05	17,060	0.05	9
Total number	319,500		28,610		
Medial geniculate body (MGB)					
Ventral subdivision of the MGB	38,700	0.04	7,590	0.04	20
Dorsal subdivision of the MGB	21,500	0.05	2,380	0.06	11
Medial subdivision of the MGB	4,900	0.04	820	0.04	17
Total number	60,200		10,790		
Auditory cortex					
Te1	227,000	0.05	23,600	0.04	10
Te2	135,500	0.05	12,650	0.05	9
Te3	153,600	0.04	17,520	0.05	12
Total number	516,100		53,770		

Mean values for Niss 1 staining have been rounded to the nearest hundred, for SMI-32 staining to the nearest ten

CE coefficient of error counted according to Gundersen et al. (1999)

the mean volumes of the SMI-32-ir neuronal somas in the same cortical layer between two adjacent cortical areas (Fig. 2). In such a case, the different orientation of neuronal somas in the same cortical layer in two adjacent cortical areas (i.e., a major source of possible bias) is highly unlikely. The volume of neurons was estimated using the nucleator technique. The use of the nucleator requires that each measured particle (e.g., cell) in the sample has a unique, arbitrary point that can be identified. For cells, the point is usually the nucleus or nucleolus. An overlay of lines was superimposed on these sections by the software (Stereo Investigator), and some points hit (ran through) the nuclei or nucleoli in the sampled neurons. Two distances (=lengths of the intercept) from the central point, e.g. the nucleolus, along the crossing line to the cell boundary were used to estimate the number-weighted mean volume. In an ideal spherical cell, the length of the intercept would be precisely the radius of the sphere; however, the operation of the nucleator technique by means of intercept lengths does not depend on the shape of the analyzed object. The volume of the SMI-32-ir soma was then calculated by averaging the third powers of the

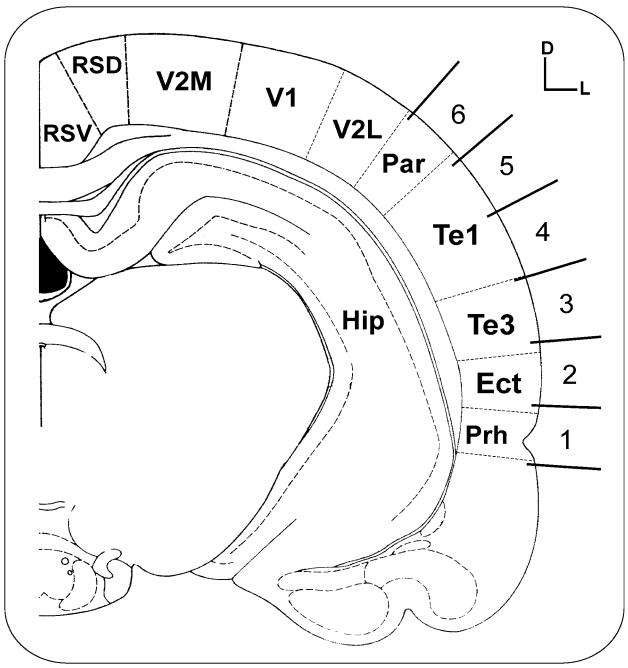

Fig. 1 Topographical overview of a coronal section through the forebrain and diencephalon (bregma −5.3 mm) and illustration of the six strips (in a section) as superimposed on the cortex (numbers *1–6*). Drawing adapted from Zilles (1985) and Paxinos and Watson (1998). *Hip* hippocampus, *Prh* perirhinal cortex, *Ect* ectorhinal cortex, *Te1* and *Te3* auditory cortex primary and secondary, *Par* parietal cortex, *V1* visual cortex primary, *V2M* and *V2L* visual cortex secondary, medial and lateral, *RSD* and *RSV* retrosplenial cortex, dorsal and ventral, *D* dorsal, *L* lateral

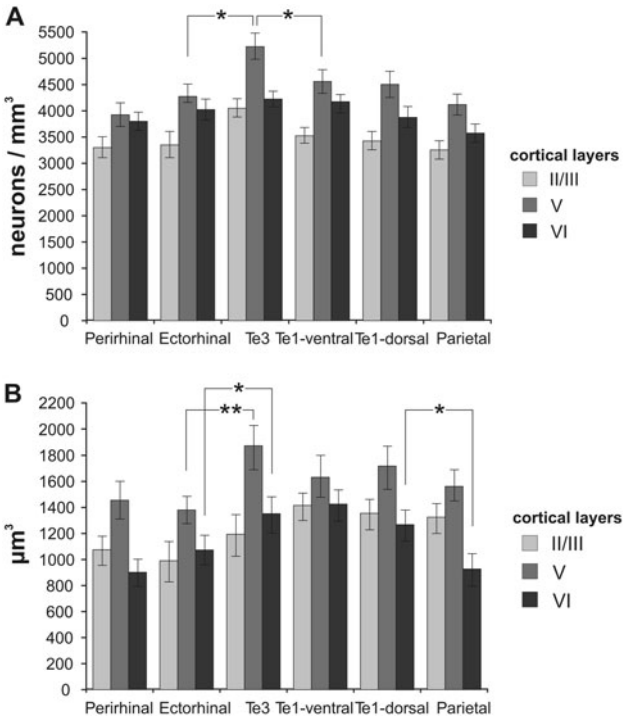

Fig. 2 Results of the quantitative evaluation of SMI-32 immunoreactivity in the cortex. **a** Numerical density of SMI-32-ir neurons and **b** average volumes of SMI-32-ir neurons in cortical layers II/III, V, and VI across the lateral cortex, including the perirhinal, ectorhinal, Te3 and Te1 auditory and parietal cortices. The *error bars* represent SEM (*$P < 0.05$, **$P < 0.01$)

intercept lengths and multiplying this average by the formula $4 \times \pi/3$ (Mayhew and Gunderesen 1996).

Statistical analysis

Only the results of the measurements of the number and volumes of SMI-32-ir neurons among adjacent cortical strips (Figs. 1, 2a, b) were statistically processed. The significance of the differences were assessed by a one-way ANOVA test and Bonferroni's multiple comparison test with the use of GraphPad Prisma software (version 4.0). *P* values of 0.05 or less were considered statistically significant.

Results

Cochlear nuclei

In the dorsal cochlear nucleus (DCN), the dense network of intensely stained neuropil made the identification of positive cells relatively difficult, especially in the darker superficial layers, while the neuropil staining within the deep core was lighter. SMI-32-ir neurons were present throughout the whole anteroposterior extent of the DCN with a slightly greater prevalence in its basal two-thirds. The immunostaining comprised neuronal somas and short segments of the variously oriented processes, some of them cut perpendicularly. In the molecular layer only a few small SMI-32-ir neurons were possible to distinguish. In the fusiform layer, middle-sized to large perikarya were found, while in the deep core of the DCN large intensely stained cells prevailed (Figs. 3a, b, 4a).

In the ventral cochlear nucleus (VCN), the number of SMI-32-ir neurons was higher when compared with the DCN. The labeled cells were present throughout the whole extent of both the posterior (PVCN) and anterior (AVCN) parts of the VCN. Large intensely stained somas prevailed in both PVCN and AVCN, and the lighter background made recognition of SMI-32-ir neurons markedly easier in comparison with DCN. The lightly stained neuropil in the VCN contained many short fragments of thick, intensely stained fibers (Figs. 3a, c, 4a).

When compared with the total number of neurons determined by Nissl staining, the SMI-32-ir cells represented 31% of the total number in the VCN and 15% in the DCN. Since the population of small granule cells, which are difficult to distinguish from glia cells and which form the majority of DCN neurons (Kulesza et al. 2002) was not

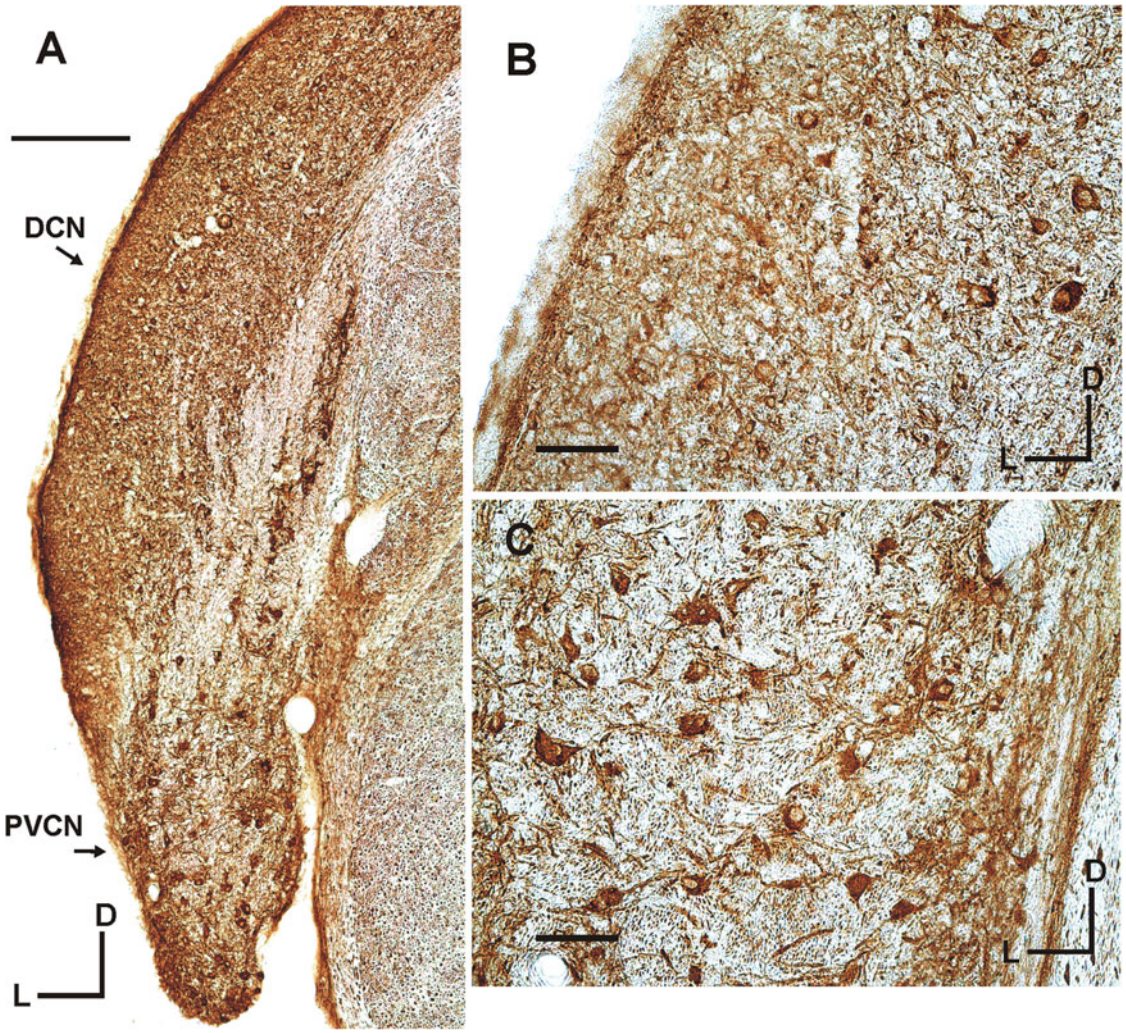

Fig. 3 SMI-32 immunoreactivity patterns in the cochlear nuclei (**a**) and at higher magnification, specifically in the dorsal (**b**) and posteroventral (**c**) cochlear nuclei—all micrographs bregma −11.4 mm. *Scale bar* **a** 200 μm, **b** 50 μm. All micrographs are from the left hemisphere. *DCN* dorsal cochlear nucleus, *PVCN* posterior part of the ventral cochlear nucleus, *D* dorsal, *L* lateral

counted in the Nissl-stained sections, the real portion of SMI-32-ir cells in this nucleus could be even lower. The difference in the percentage of SMI-32-ir neurons between the PVCN and AVCN was negligible (Table 1).

Superior olivary complex

SMI-32-ir neurons were observed in all nuclei of the SOC, and distinct inter-nuclear differences were evaluated. While in the medial nucleus of the trapezoid body (MNTB) numerous dark SMI-32-ir neurons were evident, in the lateral superior olive (LSO), medial superior olive (MSO), and periolivary nuclei, the number of immunoreactive neurons was markedly lower. In general, all the mentioned nuclei could be identified in a similar manner as in Nissl-stained sections (Fig. 5a, b).

In the MNTB, large SMI-32-ir neurons with thick basal dendrites were present through the whole extent of the MNTB. The dominant presence of SMI-32-ir cells in this nucleus was clearly recognizable to the naked eye when compared with a section stained for Nissl (Fig. 5c, d). Across the MNTB, strips of neuronal somas alternated with strips of light neuropil and bundles of fibers. The intensely labeled cells showed little variability in their staining and formed a rather uniform population (Fig. 5e). In the quantitative analysis, the immunoreactive cells constituted 58% of all neurons, thus making MNTB the only region in the rat central auditory system with a majority of SMI-32-ir neurons (Table 1).

In the LSO, positive neurons were observed through the whole extent and prevailed in the middle segment of the nucleus and near its margins (Figs. 4b, 5a). The majority of

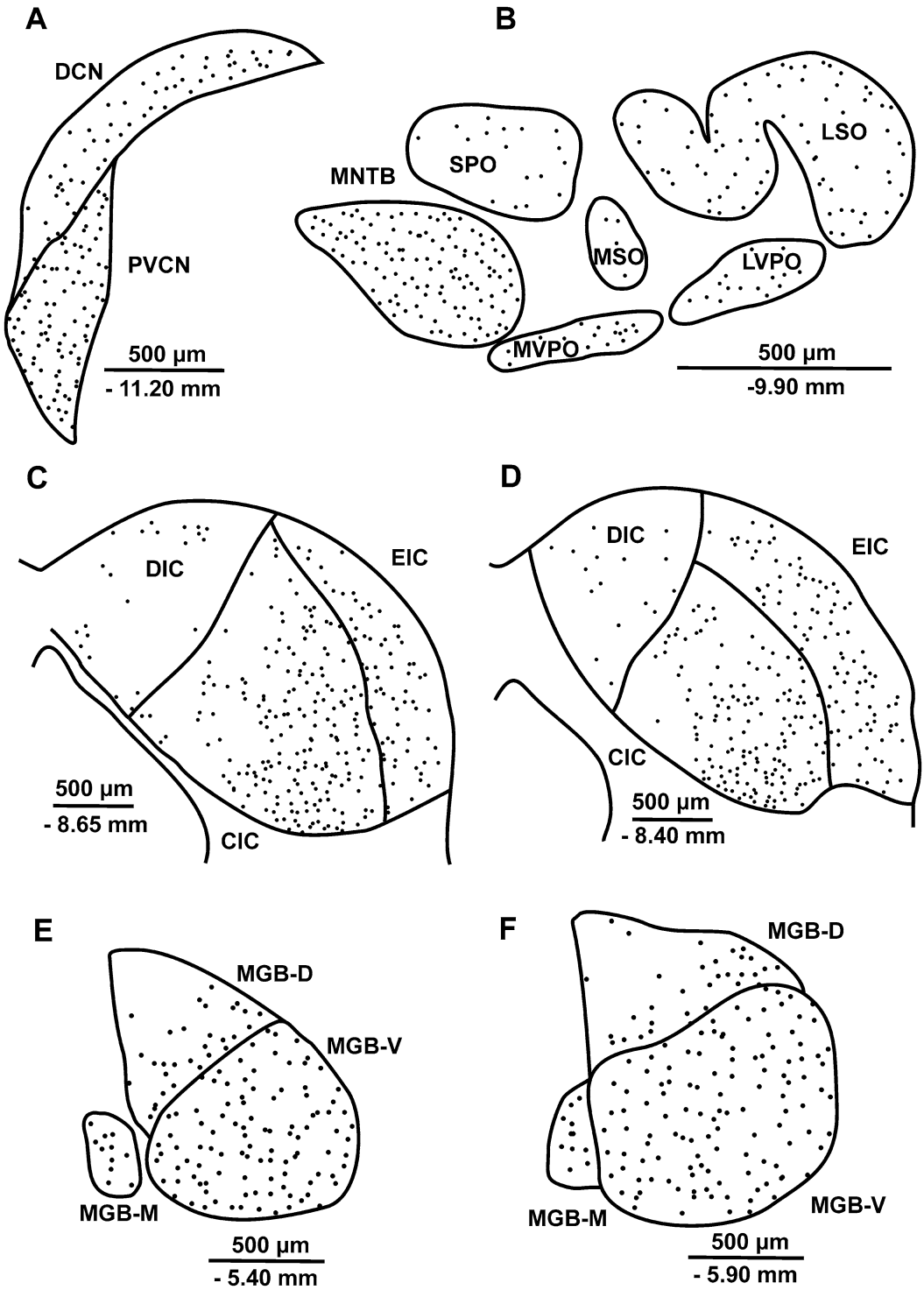

Fig. 4 Schematic illustration of the distribution of SMI-32-immunoreactive neurons in different subcortical structures: **a** cochlear nuclei; **b** superior olivary complex; **c**, **d** inferior colliculus; **e**, **f** medial geniculate body. The distance from bregma and *scale bars* is provided in each figure. **a** Left hemisphere; **b–f** right hemisphere. *DCN* dorsal cochlear nucleus, *PVCN* posterior part of the ventral cochlear nucleus, *MNTB* medial nucleus of the trapezoid body, *LSO* lateral superior olive, *MSO* medial superior olive, *SPO* superior periolivary nucleus, *LVPO* lateroventral periolivary nucleus, *MVPO* medioventral periolivary nucleus, *CIC* central nucleus of the inferior colliculus, *DIC* dorsal cortex of the inferior colliculus, *EIC* external cortex of the inferior colliculus, *MGB-V, D, M* ventral, dorsal and medial divisions of the medial geniculate body

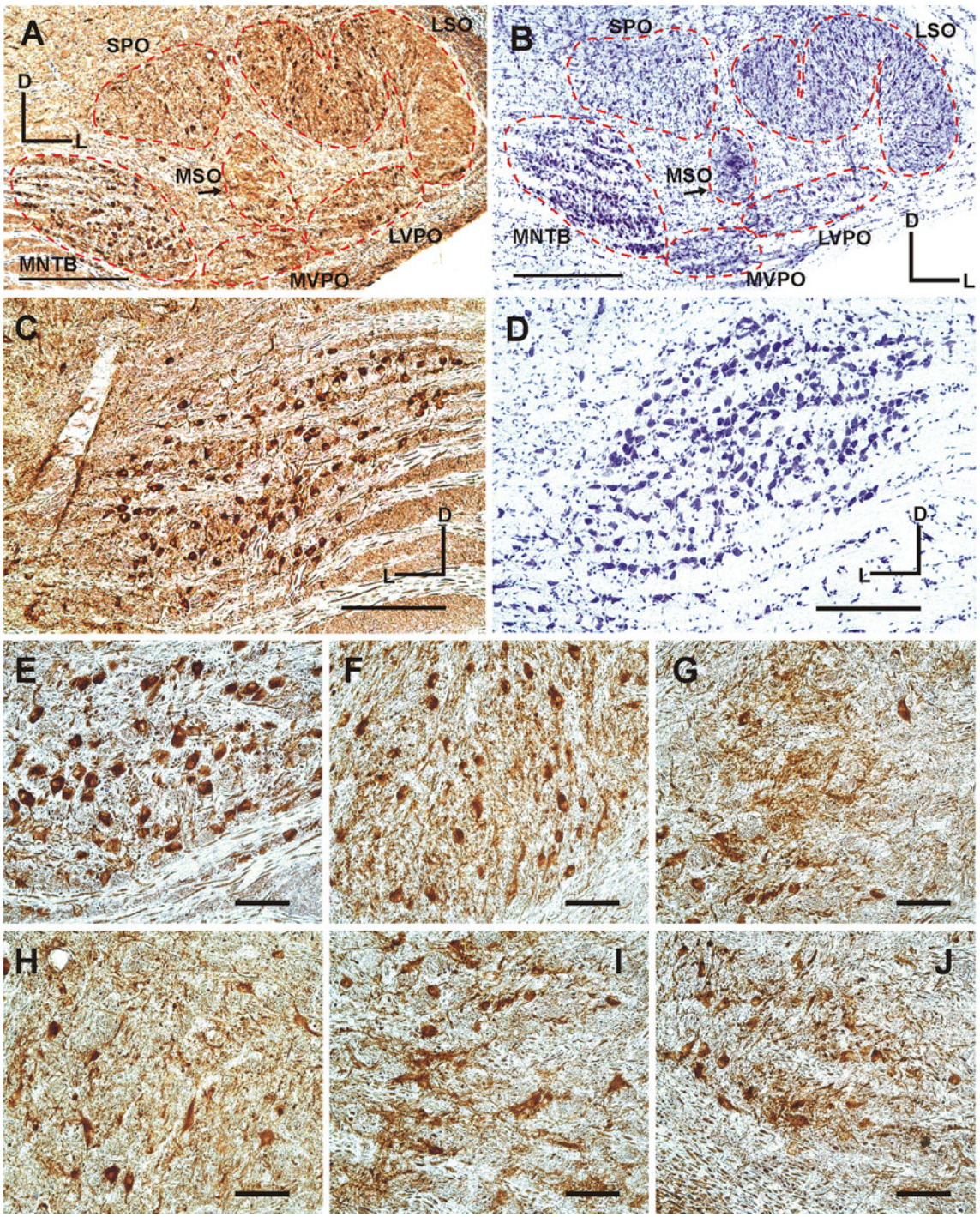

Fig. 5 Overview of the superior olivary complex in SMI-32 staining (**a**) and Nissl staining (**b**)—both bregma −9.8 mm. The nuclei in **a** and **b** are delineated with *thin dashed lines*. The dominant presence of SMI-32-ir cells in the MNTB (**c**) is demonstrated by comparison with a Nissl-stained section (**d**)—both bregma −9.8 mm. Illustration of SMI-32-immunoreactive neurons at higher magnification in the MNTB (**e**), LSO (**f**), MSO (**g**), SPO (**h**), MVPO (**i**) and LVPO (**j**). *Scale bar* **a**, **b** 500 μm; **c**, **d** 200 μm; **e**–**j** 50 μm. **a**, **b** Right hemisphere, **c**–**i** left hemisphere. *MNTB* medial nucleus of the trapezoid body, *LSO* lateral superior olive, *MSO* medial superior olive, *SPO* superior periolivary nucleus, *MVPO* medioventral periolivary nucleus, *LVPO* lateroventral periolivary nucleus, *D* dorsal, *L* lateral

labeled cells included medium-sized to large intensely stained neurons. The densely stained neuropil contained many puncta or short segments of moderately stained fibers (Fig. 5f). Labeled neurons comprised 19% of the total neuronal population. For the MSO, a dense network of positive fibers with more isolated SMI-32-ir neurons was

characteristic. Some sections with small cross-sectional profiles of the MSO contained only sparse positive neurons (Fig. 5g). The SMI-32-ir cells constituted 11% of all cells in this nucleus (Table 1).

In other periolivary nuclei, the portion of labeled cells was similar to that in the LSO. The superior periolivary nucleus (SPO) contained strongly positive cells dispersed throughout the lightly stained neuropil (Fig. 5a, h). The SMI-32-ir neurons formed 25% of all neurons. In the medioventral periolivary nucleus (MVPO) and lateroventral periolivary nucleus (LVPO), mainly strongly positive somata and darkly stained bundles of neuropil were discernible (Fig. 5a, i, j). SMI-32-ir cells in the MVPO and LVPO comprised 26 and 20% of all neurons, respectively (Table 1).

Nuclei of the lateral lemniscus

For the nuclei of the lateral lemniscus, strong SMI-32 immunoreactivity of dispersed neurons was characteristic. The cells formed vertically oriented islands within intensely stained bundles of fibers. SMI-32-immunoreactive neurons were present in all nuclei, i.e. the dorsal (DNLL), intermediate (INLL) and ventral (VNLL) nuclei (Fig. 6a, b). In comparison with Nissl-stained sections, the numerical density of SMI-32-ir neurons was apparently higher in the DNLL than in the other two nuclei. SMI-32-ir cells formed 31% of all neurons in the DNLL and 23 and 21% in the INLL and VNLL, respectively. On the other hand, the absolute number of immunoreactive neurons was highest in VNLL, which also comprised the majority of all neurons of the LL (Table 1).

Inferior colliculus

SMI-32-ir neurons were distributed throughout all three major subdivisions of the inferior colliculus with a variable intensity of immunostaining ranging from low to high. The immunostaining of the dendritic tree was not consistent, and in the case of stained dendrites, predominantly their initial segments could be traced up to a distance of 20–50 μm from the cell body (Fig. 6c, d).

In the external cortex of the inferior colliculus (EIC), the immunoreactive cells could be divided subjectively into two major groups: large dark neurons and more numerous small to middle-sized cells (Fig. 6c). No clusters of neurons or intensely stained neuropil in the second layer of the EIC, as revealed by gamma-aminobutyric acid (GABA) and glutamate decarboxylase staining (Chernock et al. 2004; Burianova et al. 2009), were visible with SMI-32 staining. In the dorsal cortex of the IC (DIC), a sparser population of small SMI-32-ir neurons was present, consisting mostly of neurons with oval and round shapes. In the central nucleus of the IC (CIC), a more polymorphous population of positive neurons in terms of their morphology, size and intensity of immunostaining was observed (Fig. 6d). The SMI-32-ir neurons were more clumped in the ventral and medial parts of the CIC, i.e. in the high-frequency region (Figs. 4c, d, 6e, f). This higher numerical density, however, corresponded to a higher density of neurons apparent in the Nissl staining of this area. In striking contrast to the lower regions of the auditory pathway, the SMI-32-ir neurons represented a significantly smaller portion of the IC neurons—10, 7, and 9% in the EIC, DIC and CIC, respectively (Table 1).

With respect to the intensity of SMI-32 immunostaining, the optical density of the immunoreactive neuropil in the CIC and EIC was higher in comparison with that of the DIC. In addition, the borders of the CIC were possible to determine on the basis of differences in the distribution and density of the labeled neurons and neuropil (Fig. 4c, d, 6e, f).

Medial geniculate body

SMI-32-ir neurons were present in all major divisions of the medial geniculate body (MGB). In the ventral division, the numerical density of SMI-32-ir cells was highest, followed by the medial division, with a markedly lower number of positive cells in the dorsal part of the MGB. In Nissl-stained sections, no significant differences in the numerical density of neurons among particular divisions of the MGB were observed. Consequently, the SMI-32-ir neurons comprised 20% of all neurons in the ventral, 17% in the medial and 11% in the dorsal divisions (Table 1).

While in the ventral and medial divisions the spatial distribution of the immunoreactive cells was rather homogenous, in the dorsal division SMI-32-ir neurons prevailed in the basal part adjacent to the ventral division. The dorsolateral parts of the dorsal division contained almost no stained cells (Fig. 7a, b). In addition, the suprageniculate nucleus was also rich in SMI-32-ir cells; however, this nucleus was not included in our stereological analysis. The distinction between particular major divisions based on SMI-32 immunoreactivity was therefore less obvious than in the IC; in particular, the transition between the ventral and dorsal divisions was rather gradual and dubious in some sections (Figs. 4e, f, 7a, b). The SMI-32-neurons in the MGB formed a population of middle-sized cells, with few larger SMI-32-ir cells present especially in the medial division. The intensity of immunostaining in SMI-32-ir somas was moderate with little variation throughout the whole MGB, and the dendritic tree was stained only occasionally with immunostaining limited to the basal dendrites (Fig. 7c–e).

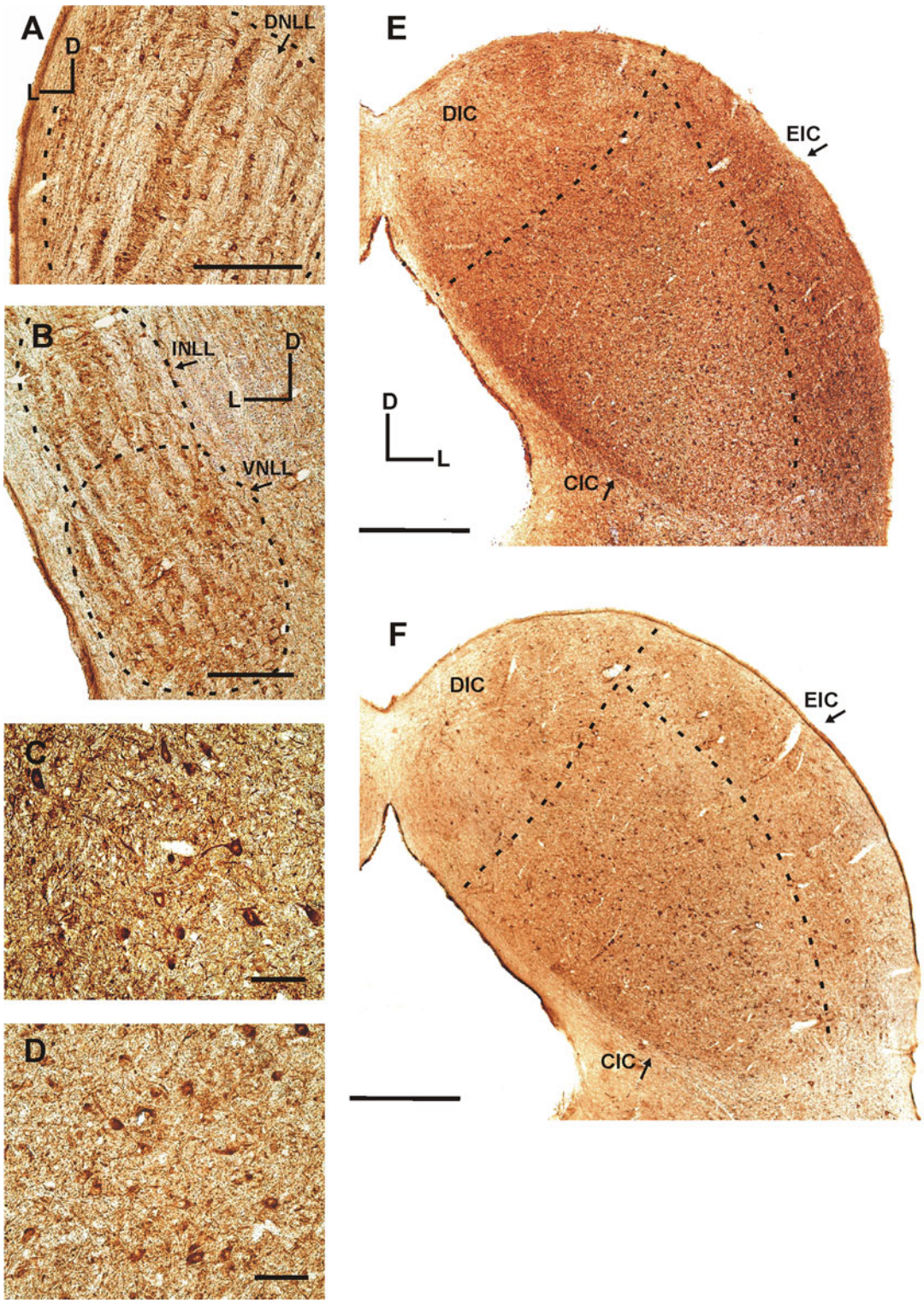

Fig. 6 SMI-32 immunoreactivity patterns in the dorsal nucleus of the LL (**a**)—bregma −8.8. mm, and the intermediate and ventral nuclei of the LL (**b**)—bregma −8.2 mm. Illustration of SMI-32-ir neurons in the external cortex of the IC (**c**), the central nucleus of the IC (**d**) and the whole IC at lower magnification captured in more (**e**) caudal (bregma −8.7 mm) and **f** rostral sections (bregma −8.45 mm). The subdivisions in **a**, **b** and **e**, **f** are marked with *thin dashed lines*. *Scale bar* **a**, **b** 200 μm; **c**, **d** 50 μm; **e**, **f** 500 μm. **a**, **b** Left hemisphere, **c**–**f** right hemisphere. *DNLL* dorsal nucleus of the lemniscus lateralis, *INLL* intermediate nucleus of the lemniscus lateralis, *VNLL* ventral nucleus of the lemniscus lateralis, *CIC* central nucleus of the inferior colliculus, *DIC* dorsal cortex of the inferior colliculus, *EIC* external cortex of the inferior colliculus, *D* dorsal, *L* lateral

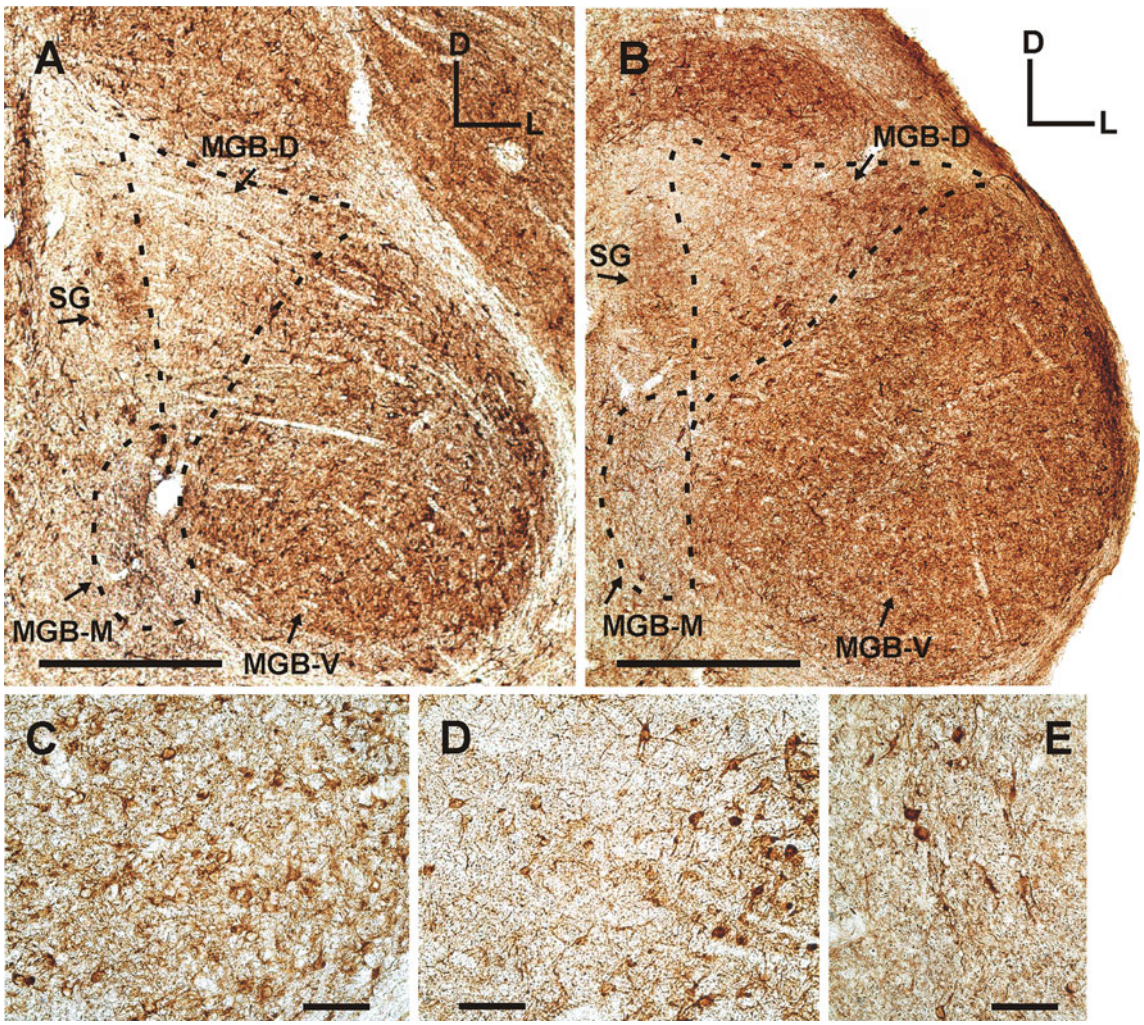

Fig. 7 SMI-32 immunoreactivity in the MGB captured in more **a** rostral (bregma −5.2 mm) and **b** caudal (bregma −5.9 mm) sections. The subdivisions in **a**, **b** are depicted with *thin dashed lines*. Note that the dorsolateral parts of the dorsal subdivision of the MGB contained almost no stained cells while the SMI-32-ir neurons are present in the parts adjacent to the ventral subdivision. Illustration of SMI-32-ir neurons at higher magnification provided in the ventral (**c**), dorsal (**d**) and medial (**e**) subdivision of the MGB. In **d**, the transition between more adjacent part (more populated by SMI-32-ir neurons) and the remote, dorsolateral, part (sparsely populated by SMI-32-ir neurons) of the dorsal subdivision of the MGB is clearly discernible. *Scale bar* **a**, **b** 400 μm; **c**, **d** 50 μm. All micrographs are from the right hemisphere. *MGB-V*, *D*, *M* ventral, dorsal and medial divisions of the medial geniculate body, *SG* suprageniculate nucleus, *D* dorsal, *L* lateral

Auditory cortex

SMI-32-ir neurons were scattered throughout cortical layers II–VI with only a few immunopositive multipolar cells and individual fibers present in layer I. In layers III and V, a relatively uniform population of intensely stained SMI-32-ir pyramidal neurons with thick immunopositive apical dendrites, sometimes extending into layer I, prevailed. Small oval granule cells were observed in layers II and IV. In layer VI, a more heterogenous population of middle-sized pyramidal or oval SMI-32-ir neurons was found, mostly with either a dominant apical dendrite or a multipolar dendritic tree with a varied orientation of the dendrites (Figs. 8a–c, 9). With the exception of the thick apical dendrites of the pyramidal neurons, which were well-stained for a distance of several hundred microns, in other labeled neurons the dendrites could be followed for a maximal distance of 50–100 μm from the cell body, and in many cases only the proximal dendrites and the basal parts of the axon were inconsistently stained.

In general, layers V and VI were the most populated, followed by layer III, with layers II and IV the least populated with SMI-32-ir cells. According to our rough estimate, in layer I only 1–2% of neurons were SMI-32-ir, while in layers II and IV they represented 5%, in layer III about 10%, in layer V 25%, and in layer VI 10% of the total neuronal population. Interestingly, most SMI-32-ir cell in layer VI were found predominantly in the VIa sublayer, while the VIb sublayer,

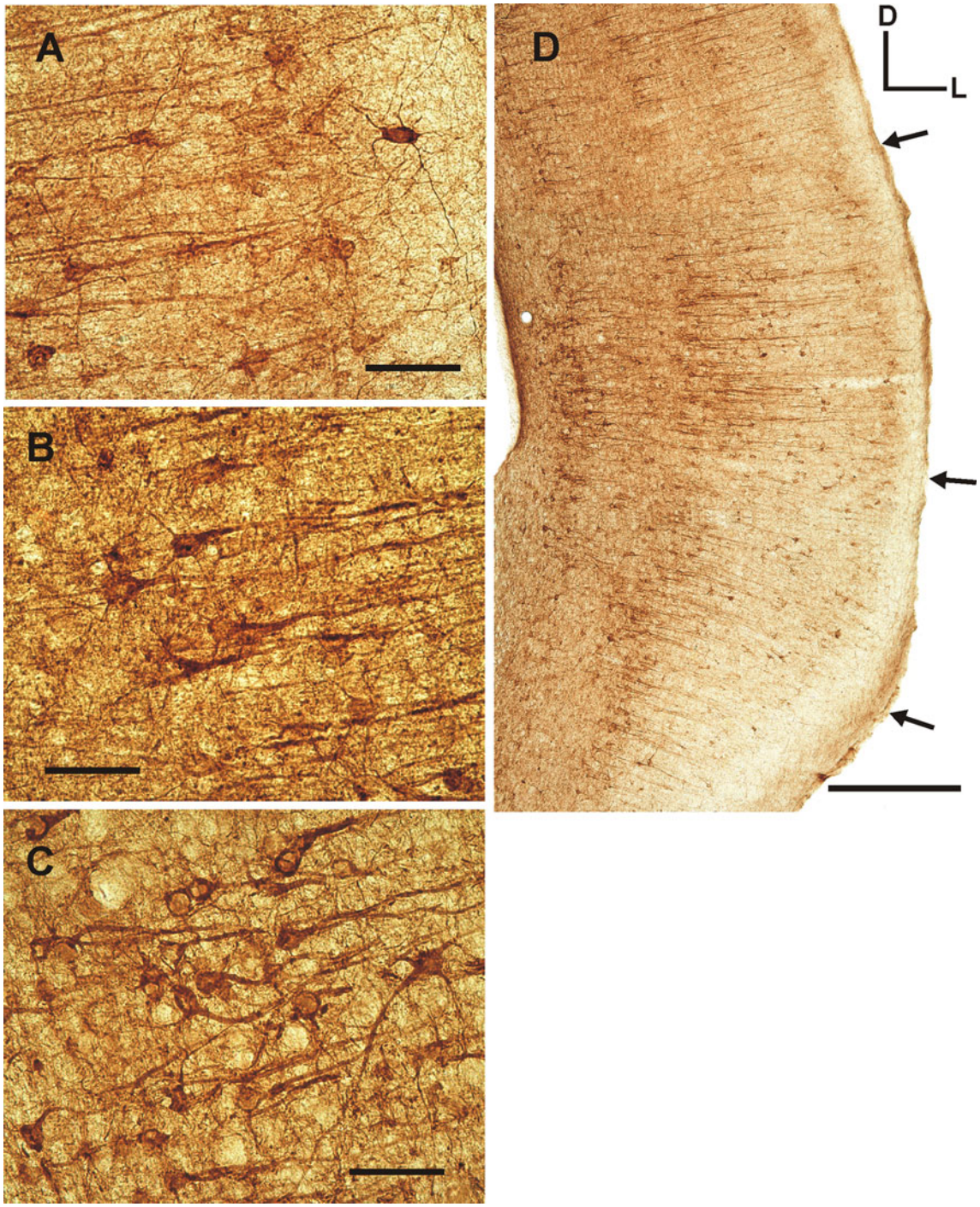

Fig. 8 Illustration of SMI-32 immunoreactivity in the auditory cortex; pyramidal neurons with thick apical dendrites in layer III of the Te1 auditory area (**a**) layer V of Te3 (**b**) and layer VI of Te3 area (**c**), and the temporal cortex (**d**, bregma −5.8 mm), with marked borders between the ectorhinal cortex and the Te3 auditory area (*lower arrow*), between the Te1 and Te3 auditory areas (*middle arrow*), and between the Te1 area and the parietal cortex (*upper arrow*). *Scale bar* **a–c** 50 µm, **d** 400 µm. All micrographs are from the right hemisphere; *D* dorsal, *L* lateral

highly populated by small neurons in Nissl staining, contained rather few SMI-32-ir cells. These general features were universally present in all examined cortical areas, also in the adjacent non-auditory cortex.

In addition, we analyzed SMI-32-ir neurons in successive strips (comprising all cortical layers), starting from the fissure rhinalis up to the parietal cortex (see Fig. 1), in order to reveal quantitative differences useful for the

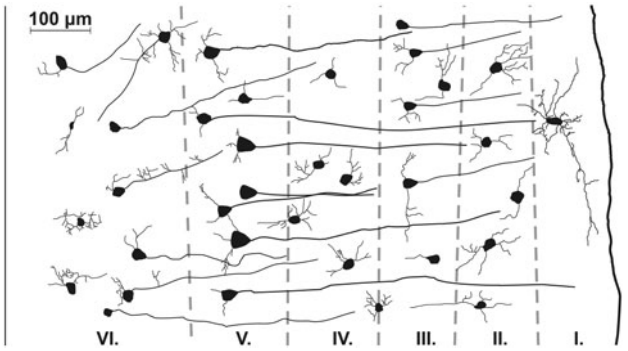

Fig. 9 Schematic illustration of the morphology of SMI-32-immunoreactive neurons throughout the cortical layers of the Te1 auditory area. The illustration shows the different neuronal types represented in particular cortical layers, including pyramidal neurons (layers III, V and the superficial part of layer VI) with long and thick apical dendrites often extending into layer I. The numerical density of neurons and neuronal types in particular layers is not proportional nor is the relative thickness of the layers (especially layer VI)

parcellation of the auditory (as well as the surrounding non-auditory) cortex. Statistically significant differences were evident between the Te3 auditory cortex and the ventrally situated ectorhinal and perirhinal non-auditory areas. The numerical density and average volumes of SMI-32-immunoreactive neurons and the optical density of the neuropil were higher in the Te3 auditory area compared to the ventrally situated cortex ($P < 0.05$). The differences were most pronounced in the population of layer V SMI-32-ir pyramidal neurons ($P < 0.01$). The upper borders of the Te1 area were possible to ascertain on the basis of decreased SMI-32 immunoreactivity of the neuropil in layers II/III and VI (Fig. 8d). However, the dorsal transition was gradual towards the parietal, somatosensory or secondary visual cortices, was accompanied by only a slow decrease in the numerical density and volume of SMI-32-ir neurons, and was therefore less pronounced when compared to the ectorhinal-Te3 borders (Fig. 2). In contrast, the average immunostaining intensity of the neuronal somas was similar across the auditory and surrounding non-auditory areas as well as across the cortical layers.

Within the auditory cortex, the traditional Te1, Te3 and Te2 areas (Zilles 1985) were possible to distinguish on the basis of the variable numerical density and volumes of SMI-32-ir neurons. These differences were especially visible in layer V. The highest numerical density and largest somas of SMI-32-ir neurons were found in the ventral associative Te3 area, followed by the caudal associative Te2 area and the auditory core (Te1). No other auditory areas, as shown in other rat atlases (Paxinos and Watson 1998) or suggested by new detailed electrophysiological mapping (Polley et al. 2007), were possible to differentiate.

While the differences in the number and size of SMI-32-ir neurons between the Te1 and Te3 auditory areas were statistically significant ($P < 0.05$; Fig. 2), the quantitative differences between the caudal associative Te2 auditory area and the Te1 or Te3 area were not. However, the boundaries of the Te2 and Te3 areas vs. Te1 area could be delineated on the basis of stronger neuropil immunopositivity in layers II/III, V (inconsistently) and VI of the rat auditory core (Te1). The transition between the Te3 and Te2 areas was more gradual and less visible. Compared with the Nissl-stained sections, SMI-32-ir cells formed 10% of all neurons in the Te1 auditory core, 12% in the Te3 auditory area and 9% in the Te2 area (Table 1). The portions of SMI-32-ir cells in individual cortical layers represented a rough estimate with a high coefficient of error; therefore, the results of this brief survey were not included into Table 1.

Discussion

Our results demonstrate that SMI-32 immunoreactivity is present in all examined parts of the central auditory system; however, except for the MNTB, in all structures SMI-32-ir neurons represent only a minor portion of all neurons. While subcortical auditory structures have been only marginally examined for SMI-32 immunoreactivity so far, the results obtained in the auditory cortex need to be interpreted in the context of previous findings. In the mammalian cerebral cortex, SMI-32 immunoreactivity was reported to be predominant for type I pyramidal cortical neurons (Sternberger and Sternberger 1983; Campbell and Morrison 1989; Voelker et al. 2004). Type I pyramidal neurons have long apical dendrites extending into layer I and projecting to subcortical regions, while type II neurons have apical dendrites, which arborize in layers II–IV and make cortico-cortical projections. The neurofilament content is thought to be necessary for structural stability and to be involved in nutrition transport in large, fast firing neurons with long processes (Goldstein et al. 1987; Lasek 1988). In addition, the immunoreactivity of heavy non-phosphorylated neurofilaments labeled by SMI-32 in neurons is believed to be associated with the extent of axonal myelination and with increases in soma size (Campbell and Morrison 1989; Tsang et al. 2000; Kirkcaldie et al. 2002). This suggestion may be supported by findings in the cat lateral geniculate body under conditions of early visual deprivation. A significant decrease in the volume of neuronal somas, a reduction in dendritic trees, and a loss of neurofilament content were found in deprived neurons in comparison with their non-deprived counterparts (Duffy and Slusar 2009). In agreement with this hypothesis, SMI-32-ir cells observed in our experiment were above average sized neurons in the majority of analyzed auditory structures (in comparison with Nissl-stained sections), including the auditory cortex.

The cochlear nuclei have been widely examined for other neurochemical markers, e.g. for calcium binding proteins and the expression of major neurotransmitters and receptor subunits (Altschuler et al. 1986; Idrizbegovic et al. 2001, 2004; Alibardi 2003; Luján et al. 2004; Fredrich et al. 2009). In our findings, SMI-32-positive neurons prevailed in the ventral cochlear nucleus, while the dorsal nucleus contained a lower number of labeled neurons located predominantly in the deep layers. The different representation of SMI-32-ir neurons in the VCN and DCN may reflect differences in the projection and function of these nuclei (Bajo et al. 1993; Alibardi 1998, 2003; Cant and Benson 2003). In the VCN, the SMI-32-ir cells constituted roughly one-third of all neurons, which suggests the importance of heavy neurofilament subunits in the neurons of the VCN. The mammalian VCN contains six to seven major established cell types (Malmierca 2003; Cant and Benson; 2003). In our immunostaining, the types of SMI-32-ir neurons could not be clearly distinguished, though their morphology was sometimes reminiscent of multipolar or bushy cells. In addition, though we did not run stereological probes to measures the mean volumes of the neurons (mainly for methodological reasons—see "Materials and methods", "Microscopy"). In a survey we could observe that the SMI-32-ir neurons in both the VCN and DCN were mainly cells with above average neuronal volumes in comparison with those seen in Nissl-stained cochlear nuclei.

Due to the intensely stained background in the DCN, the identification of the morphological types of the stained neurons in this nucleus was even less easy. In the DCN, the portion of SMI-32-ir cells was markedly low, especially in the superficial molecular layer rich in small granular cells. The high staining intensity of the background neuropil in the molecular layer might have obscured our identification of a few mildly stained SMI-32-ir cells; however, the influence of their absence on the total number of SMI-32-ir neurons in the DCN would be negligible. The SMI-32-ir cells were mainly present in the fusiform and deep layers, which are known to be the source of projections to the IC (Cant and Benson 2003).

In the superior olivary complex, SMI-32 immunoreactivity has been examined in man (Bazwinsky et al. 2003). However, the structure and function of the SOC is very different in humans and in rodents and therefore not easy to compare (Moore and Moore 1971; Kulesza 2007). In the rat superior olivary complex, several neuronal types have been described with Nissl staining, immunostaining for calcium binding proteins or glutamate decarboxylase (Friauf 1994; Rietzel and Friauf 1998; Malmierca 2003; Fredrich et al. 2009). In the SMI-32 immunostaining, a correspondence with the established neuronal types was not possible to find in most cases, especially not in the LSO with its diverse neuronal populations (Malmierca 2003; Fredrich et al. 2009). The notable exceptions were formed by the MNTB and SPO.

In general, striking differences were observed between the MNTB on one side, with approximately 60% of SMI-32 labeled cells, and all other nuclei of the superior olivary complex, with 15–25% of labeled neurons only. The reason for the markedly higher proportion of SMI-32-ir neurons in the MNTB is not clear although it might be associated with the different functions and connections of the neurons in this nucleus. In contrast to neurons in other nuclei of the superior olivary complex, the neurons in the MNTB receive their excitatory input through very large somatic terminals, the calyces of Held (Kuwabara et al. 1991; von Gersdorff and Borst 2002; Schneggenburger and Forsythe 2006), and send glycinergic inhibitory projections, predominantly into the LSO (Moore and Caspary 1983; Wu and Kelly 1991, 1995; Sanes and Friauf 2000). The large calyciform input is suggested to provide high conservation of temporal precision as excitation is translated to inhibition (Wu and Kelly 1993; Taschenberger and von Gersdorff 2000). Furthermore, the principal neurons in the MNTB are highly metabolically active cells with thick myelinated fast-conducting axons, exhibiting high firing rates, projecting collaterals into several targets besides the LSO (Kuwabara and Zook 1991; Sommer et al. 1993; Smith et al. 1998; Kopp-Scheinpflug et al. 2008) and also possessing retrograde glycinergic inhibition capable of suppressing calyceal transmission (Awatramani et al., 2004). Such a situation corresponds with the hypothesis suggested above for the cortical SMI-32-ir neurons, i.e. that the larger the neuronal soma and the more myelinated the axons in projecting neurons, the more likely are these neurons to be SMI-32-immunopositive (Lasek 1988; Tsang et al. 2000; Kirkcaldie et al. 2002; Mellott et al. 2010).

In the SPO, more than 90% of all neurons are known to be GABAergic and projecting into the IC (Kulesza and Berrebi 2000; Saldaña et al. 2009); therefore, we may suggest that at least part of the observed SMI-32-ir cells (25% of all neurons) belonged to this type.

In coronal sections, the rostral and caudal borders between the LSO, LVPO and MVPO were to some extent difficult to distinguish in both the Nissl and SMI-32 stainings. This fact could explain the discrepancy in the reported absolute number of neurons (Nissl staining) for the mentioned structures between our results and the results reported by Kulesza et al. (2002), which otherwise are in relatively good agreement (despite the different strains of rats used, Wistar vs. Long Evans). Specifically, Kulesza et al. (2002) reported a higher number of neurons in the LVPO (LNTB) and MVPO (VNTB) and a lower number in the LSO. However, if combined, the sum of neurons in the LSO, MVPO and LVPO is similar in both reports. In

addition, the portion of SMI-32-ir neurons in these nuclei, as revealed in our staining, was also relatively similar (LSO 19%, LVPO 20%, MVPO 26%), therefore the uncertainty in determining precise topographical borders should not be critical for the reported occurrence of SMI-32-ir neurons.

In the nuclei of the lateral lemniscus, a dominant presence of inhibitory GABAergic neurons has been described. In the VNNL and INLL, two-thirds of neurons are GABAergic (Riquelme et al. 2001); consequently, we cannot confirm or exclude whether this population overlaps with that of SMI-32-ir neurons, which form less than one-fourth of all neurons in these nuclei. On the other hand, almost all neurons in the DNLL are GABAergic and projecting to the IC (Zhang et al. 1998; Ueyama et al. 1999), which strongly suggests at least a partial overlap with SMI-32-ir cells, since they constitute about one-third of all cells on the basis of our results. The functional implications of such a specific neuronal subpopulation in an otherwise relatively homogenous nucleus remain, similarly as for the SPO, to be elucidated.

In the inferior colliculus, SMI-32-ir neurons were present in all three major subdivisions (Paxinos and Watson 1998); however, they constituted a significantly smaller portion of the total number of neurons when compared with the lower parts of the auditory pathway. Furthermore, the portion of SMI-32-ir neurons in the IC was also lower in comparison with the MGB. In contrast, the total number of neurons in the rat IC is by far the highest among all subcortical auditory nuclei, as shown by our results and those of Kulesza et al. (2002). Consequently, the absolute number of SMI-32-ir neurons in the IC was higher than in the cochlear nuclei, superior olivary complex or MGB; however, this divergence was less pronounced than that in the absolute number of all neurons (Table 1).

Although both the CIC and ventral MGB are parts of the primary tonotopic auditory pathway, SMI-32-ir neurons in the ventral division of the MGB constituted a markedly larger portion of all neurons. However, there are significant differences in the representation of other markers between the IC and MGB in rodents, which might partially explain this discrepancy; for example, GABAergic neurons are very rare in the MGB, while they form a significant portion (25–30%) of all neurons in the IC (Winer and Larue 1996; Merchán et al. 2005). In contrast to the MGB, a considerable portion of the neurons in the rat IC is thought to consist of local circuit neurons (Oliver et al. 1991).

Furthermore, the dorsal division of the MGB could be further divided on the basis of SMI-32 staining into two parts, an outer distal part with very few positive cells and very low optical density of the neuropil and a thinner deep part (adjacent to the ventral MGB) with only a slightly lower density of SMI-32 cells in comparison with the ventral division of the MGB. No such inner borders within the dorsal division of the MGB were clearly visible in the Nissl staining of our material. This delineation may, however, correspond to a subdivision distinguished by Winer et al. (1999). The authors differentiated several subnuclei in the dorsal MGB. Specifically, the outer superficial part of the dorsal MGB in our immunostaining might correspond to the dorsal superficial and dorsal sub-nuclei and the adjacent deep part to the deep sub-dorsal nucleus (Winer et al. 1999). Nevertheless, all these sub-nuclei of the dorsal MGB are known in the cat to send projections to the non-tonotopic auditory and multisensory cortical areas (Lee and Winer 2008a). In contrast to the outer part, the deep part of the dorsal MGB is thought to be influenced by projections from the Te1 auditory area (Hazama et al. 2004). To some extent, a similar immunoreactivity pattern of SMI-32 was found in the simian lateral geniculate body, with intensely stained magnocellular layers (related to the fast-conducting pathway) and less stained parvocellular layers (Chaudhuri et al. 1996; Bourne and Rosa 2003; Soares et al. 2008).

At the cortical level, we found significant differences in the representation of SMI-32-ir neurons among particular cortical layers. Such differences were reported by several other authors with predominant SMI-32-immunoreactivity found in the pyramidal cells of layers II/III, V and VI in the neocortex of mammals (Sternberger and Sternberger 1983; Voelker et al. 2004; Molnár and Cheung 2006; Soares et al. 2008; Lee and Winer 2008b, c). However, although SMI-32 staining was prevalent in pyramidal neurons in our findings, it was not limited to them, and a considerable number of non-pyramidal multipolar and granular cells was also labeled, mostly in layers IV and VI. In addition, we observed a relatively numerous population of labeled SMI-32-ir cells in layer VIa, in agreement with previous observations in monkeys and cats (Soares et al. 2008; Mellott et al. 2010), however in disagreement with the figures shown in the published chemoarchitectonic atlas of the rat for SMI-32 immunostaining (Paxinos et al. 1998a, b). The reason for this discrepancy is not clear; nevertheless, the relatively high presence of SMI-32-ir neurons in layer VIa was maintained in most sections of all the stained brains in our material and false positivity was excluded ("Methods"). In addition, possible strain differences should be taken into account, since Long Evans rats were analyzed in our present experiments, while Paxinos et al. (1998a, b) used Wistar rats.

From the quantitative point of view, it should be noted that only a small portion of cerebral neurons is SMI-32-positive. According to the rough estimates of other authors, such cells represent approximately 10–20% of all cortical neurons (Voelker et al. 2004). Our data, based on a comparison with the number of Nissl-stained neurons, show

that only about 10% of all neurons in the auditory cortex (all layers, I–VI) are SMI-32-positive with negligible differences between the Te1, Te2 and Te3 areas. In layer V, which is the major source of the descending projections from the auditory cortex (Herbert et al. 1991; Winer and Prieto 2001), the portion of SMI-32-ir cells was significantly higher but still comprised only about 25% of all layer V neurons. In layer VI, SMI-32 labeled neurons with a predominantly pyramidal morphology. The pyramidal neurons of layer VI are known to be another source of subcortical projections (Prieto and Winer 1999). On the other hand, small non-pyramidal cells in the deeper VIb layer were largely not SMI-32-positive in our material, and these cells have been suggested to be mainly excitatory but corticocortical projecting neurons (Prieto and Winer 1999; Andjelic et al. 2009).

In addition, we found limited inter-areal differences in the number and volumes of SMI-32-ir neurons. These findings are in agreement with previous reports in which the pattern of SMI-32 immunoreactivity was successfully used for the parcellation of the auditory, visual, somatosensory and prefrontal cortical areas in mammalian species such as gerbils (Budinger et al. 2000; Bajo and Moore 2005), hamsters (Boire et al. 2005), rats (Van De Werd and Uylings 2008), cats (Van der Gucht et al. 2001, Mellott et al. 2010), tree shrews (Wong and Kaas 2009) and primates (Baldauf 2005). Interestingly, in agreement with our results obtained in the rat auditory cortex, Baldauf (2005) found in marmosets a higher number of SMI-32-ir neurons in the associative cortical areas in comparison with the primary visual cortex, and Wong and Kaas (2008) observed in gray squirrels larger SMI-32-ir cells in layer V of the secondary visual areas compared to the primary visual cortex. On the other hand, in the majority of reports involving SMI-32 immunostaining, the number of differentiated cortical areas is limited. Our quantitative analysis of neuronal numbers and volumes shows limits as well. The quantitative differences among cortical auditory fields (Te1, Te2, Te3) demonstrated in our results are rather subtle even if statistically significant, and the possible functional implications of such differences need further clarification.

In summary, SMI-32-ir neurons apparently constitute a significant but minor neuronal population in all examined auditory regions with the exception of the MNTB. Interestingly, according to Nissl staining, the differences in the total number of all neurons among subcortical auditory levels (CN, SOC, LL, IC, MGB) are more pronounced than the differences in the total number of SMI-32-ir neurons. In addition, the abundant presence of SMI-32-immunoreactivity in the MNTB may suggest a specific role for heavy non-phosphorylated neurofilaments in the neurons of this nucleus. At the cortical level, SMI-32-immunoreactivity was prevalent in, but not limited to, pyramidal cells with long apical dendrites. Moreover, in layer V, the main source of subcortical projections, the percentage of SMI-32-ir neurons was similar to that observed in the subcortical nuclei, which are parts of the tonotopic ascending pathway. On the other hand, the differences among cortical areas were more subtle, though they allow the delineation of the auditory areas from the non-auditory cortex and the central auditory core from the associative auditory areas.

Acknowledgments The authors wish to thank Mrs. J. Janouskova for her technical assistance. This study was supported by the Grant Agency of the Czech Republic (309/07/1336), AV0Z50390512 and LC 554.

References

Alibardi L (1998) Ultrastructural and immunocytochemical characterization of neurons in the rat ventral cochlear nucleus projecting to the inferior colliculus. Ann Anat 180:415–426

Alibardi L (2003) Ultrastructural distribution of glycinergic and GABAergic neurons and axon terminals in the rat dorsal cochlear nucleus, with emphasis on granule cell areas. J Anat 203:31–56

Altschuler RA, Hoffman DW, Wenthold RJ (1986) Neurotransmitters of the cochlea and cochlear nucleus: immunocytochemical evidence. Am J Otolaryngol 7:100–106

Andersen BB, Gundersen HJG (1999) Pronounced loss of cell nuclei and anisotropic deformation of thick sections. J Microsc 196:69–73

Andjelic S, Gallopin T, Cauli B, Hill EL, Roux L, Badr S, Hu E, Tamás G, Lambolez B (2009) Glutamatergic nonpyramidal neurons from neocortical layer VI and their comparison with pyramidal and spiny stellate neurons. J Neurophysiol 101:641–654

Ashwell KW (2008) Topography and chemoarchitecture of the striatum and pallidum in a monotreme, the short-beaked echidna (*Tachyglossus aculeatus*). Somatosens Mot Res 25:171–187

Awatramani GB, Turecek R, Trussell LO (2004) Inhibitory control at a synaptic relay. J Neurosci 24:2643–2647

Bajo VM, Moore DR (2005) Descending projections from the auditory cortex to the inferior colliculus in the gerbil, Meriones unguiculatus. J Comp Neurol 486:101–116

Bajo VM, Merchán MA, López DE, Rouiller EM (1993) Neuronal morphology and efferent projections of the dorsal nucleus of the lateral lemniscus in the rat. J Comp Neurol 334:241–262

Baldauf ZB (2005) SMI-32 parcellates the visual cortical areas of the marmoset. Neurosci Lett 383:109–114

Bazwinsky I, Hilbig H, Bidmon HJ, Rübsamen R (2003) Characterization of the human superior olivary complex by calcium binding proteins and neurofilament H (SMI-32). J Comp Neurol 456:292–303

Bickford ME, Guido W, Godwin DW (1998) Neurofilament proteins in Y-cells of the cat lateral geniculate nucleus: normal expression and alteration with visual deprivation. J Neurosci 18:6549–6557

Boire D, Desgent S, Matteau I, Ptito M (2005) Regional analysis of neurofilament protein immunoreactivity in the hamster's cortex. J Chem Neuroanat 29:193–208

Bourne JA, Rosa MG (2003) Laminar expression of neurofilament protein in the superior colliculus of the marmoset monkey (*Callithrix jacchus*). Brain Res 973:142–145

Budinger E, Heil P, Scheich H (2000) Functional organization of auditory cortex in the *Mongolian gerbil* (*Meriones unguiculatus*) III. Anatomical subdivisions and corticocortical connections. Eur J Neurosci 12:2425–2451

Burianova J, Ouda L, Profant O, Syka J (2009) Age-related changes in GAD levels in the central auditory system of the rat. Exp Gerontol 44:161–169

Campbell MJ, Morrison JH (1989) Monoclonal antibody to neurofilament protein (SMI-32) labels a subpopulation of pyramidal neurons in the human and monkey neocortex. J Comp Neurol 282:191–205

Cant NB, Benson CG (2003) Parallel auditory pathways: projection patterns of the different neuronal populations in the dorsal and ventral cochlear nuclei. Brain Res Bull 60:457–474

Chaudhuri A, Zangenehpour S, Matsubara JA, Cynader MS (1996) Differential expression of neurofilament protein in the visual system of the vervet monkey. Brain Res 709:17–26

Chernock ML, Larue DT, Winer JA (2004) A periodic network of neurochemical modules in the inferior colliculus. Hear Res 188:12–20

Cudkowicz M, Kowall NW (1990) Degeneration of pyramidal projection neurons in Huntington's disease cortex. Ann Neurol 27:200–204

Duffy KR, Slusar JE (2009) Monocular deprivation provokes alteration of the neuronal cytoskeleton in developing cat lateral geniculate nucleus. Vis Neurosci 26:319–328

Fredrich M, Reisch A, Illing RB (2009) Neuronal subtype identity in the rat auditory brainstem as defined by molecular profile and axonal projection. Exp Brain Res 195:241–260

Friauf E (1994) Distribution of calcium-binding protein calbindin-D28k in the auditory system of adult and developing rats. J Comp Neurol 349:193–211

Goldstein ME, Sternberger LA, Sternberger NH (1987) Varying degrees of phosphorylation determine microheterogeneity of the heavy neurofilament polypeptide (Nf-H). J Neuroimmunol 14: 135–148

Gundersen HJG, Jensen EBV, Kieu K, Nielsen J (1999) The efficiency of systematic sampling in stereology-reconsidered. J Microsc 193:199–211

Hassiotis M, Paxinos G, Ashwell KW (2004) Cyto- and chemoarchitecture of the cerebral cortex of the Australian echidna (Tachyglossus aculeatus) I. Areal organization. J Comp Neurol 475:493–517

Hazama M, Kimura A, Donishi T, Sakoda T, Tamai Y (2004) Topography of corticothalamic projections from the auditory cortex of the rat. Neuroscience 124:655–667

Herbert H, Aschoff A, Ostwald J (1991) Topography of projections from the auditory cortex to the inferior colliculus in the rat. J Comp Neurol 304:103–122

Hof PR, Morrison JH (1990) Quantitative analysis of a vulnerable subset of pyramidal neurons in Alzheimer's disease: II. Primary and secondary visual cortex. J Comp Neurol 301:55–64

Hoffman PN, Cleveland DW, Griffin JW, Landes PW, Cowan NJ, Price DL (1987) Neurofilament gene expression: a major determinant of axonal caliber. Proc Natl Acad Sci USA 84:3472–3476

Idrizbegovic E, Canlon B, Bross LS, Willott JF, Bogdanovic N (2001) The total number of neurons and calcium binding protein positive neurons during aging in the cochlear nucleus of CBA/CaJ mice: a quantitative study. Hear Res 158:102–115

Idrizbegovic E, Bogdanovic N, Willott JF, Canlon B (2004) Age-related increases in calcium-binding protein immunoreactivity in the cochlear nucleus of hearing impaired C57BL/6J mice. Neurobiol Aging 25:1085–1093

Irvine KA, Blakemore WF (2006) Age increases axon loss associated with primary demyelination in cuprizone-induced demyelination in C57BL/6 mice. J Neuroimmunol 175:69–76

Kirkcaldie MT, Dickson TC, King CE, Grasby D, Riederer BM, Vickers JC (2002) Neurofilament triplet proteins are restricted to a subset of neurons in the rat neocortex. J Chem Neuroanat 24:163–171

Kopp-Scheinpflug C, Tolnai S, Malmierca MS, Rübsamen R (2008) The medial nucleus of the trapezoid body: comparative physiology. Neuroscience 154:160–170

Kulesza RJ Jr (2007) Cytoarchitecture of the human superior olivary complex: medial and lateral superior olive. Hear Res 225:80–90

Kulesza RJ Jr, Berrebi AS (2000) Superior paraolivary nucleus of the rat is a GABAergic nucleus. J Assoc Res Otolaryngol 1:255–269

Kulesza RJ, Viñuela A, Saldaña E, Berrebi AS (2002) Unbiased stereological estimates of neuron number in subcortical auditory nuclei of the rat. Hear Res 168:12–24

Kuwabara N, Zook JM (1991) Classification of the principal cells of the medial nucleus of the trapezoid body. J Comp Neurol 314:707–720

Kuwabara N, DiCaprio RA, Zook JM (1991) Afferents to the medial nucleus of the trapezoid body and their collateral projections. J Comp Neurol 314:684–706

Lasek RJ (1988) Studying the intrinsic determinants of neuronal form and function. In: Lasek RJ, Black MM (eds) Intrinsic determinants of neuronal form and fiction. Alan R. Liss, New York, pp 1–60

Lawson SN, Waddell PJ (1991) Soma neurofilament immunoreactivity is related to cell size and fibre conduction velocity in rat primary sensory neurons. J Physiol 435:41–63

Lee MK, Cleveland DW (1994) Neurofilament function and dysfunction: involvement in axonal growth and neuronal disease. Curr Opin Cell Biol 6:34–40

Lee CC, Winer JA (2008a) Connections of cat auditory cortex: I. Thalamocortical system. J Comp Neurol 507:1879–1900

Lee CC, Winer JA (2008b) Connections of cat auditory cortex: II. Commissural system. J Comp Neurol 507:1901–1919

Lee CC, Winer JA (2008c) Connections of cat auditory cortex: III. Corticocortical system. J Comp Neurol 507:1920–1943

Luján R, Shigemoto R, Kulik A, Juiz JM (2004) Localization of the GABAB receptor 1a/b subunit relative to glutamatergic synapses in the dorsal cochlear nucleus of the rat. J Comp Neurol 475:36–46

Luppino G, Hamed SB, Gamberini M, Matelli M, Galletti C (2005) Occipital (V6) and parietal (V6A) areas in the anterior wall of the parieto-occipital sulcus of the macaque: a cytoarchitectonic study. Eur J Neurosci 21:3056–3076

Malmierca MS (2003) The structure and physiology of the rat auditory system: an overview. Int Rev Neurobiol 56:147–211

Mancardi G, Hart B, Roccatagliata L, Brok H, Giunti D, Bontrop R, Massacesi L, Capello E, Uccelli A (2001) Demyelination and axonal damage in a non-human primate model of multiple sclerosis. J Neurol Sci 184:41–49

Mayhew TM, Gunderesen HJG (1996) 'If you assume, you can make an ass out of u and me': a decade of the dissector for stereological counting of particles in 3D space. J Anat 188:1–15

Mellott JG, Van der Gucht E, Lee CC, Carrasco A, Winer JA, Lomber SG (2010) Areas of cat auditory cortex as defined by neurofilament proteins expressing SMI-32. Hear Res 267:119–136

Merchán M, Aguilar LA, Lopez-Poveda EA, Malmierca MS (2005) The inferior colliculus of the rat: quantitative immunocytochemical study of GABA and glycine. Neuroscience 136:907–925

Molnár Z, Cheung AF (2006) Towards the classification of subpopulations of layer V pyramidal projection neurons. Neurosci Res 55:105–115

Moore MJ, Caspary DM (1983) Strychnine blocks binaural inhibition in lateral superior olivary neurons. J Neurosci 3:237–242

Moore JK, Moore RY (1971) A comparative study of the superior olivary complex in the primate brain. Folia Primatol (Basel) 16:35–51

Morel A, Loup F, Magnin M, Jeanmonod D (2002) Neurochemical organization of the human basal ganglia: anatomofunctional territories defined by the distributions of calcium-binding proteins and SMI-32. J Comp Neurol 443:86–103

Oliver DL, Kuwada S, Yin TC, Haberly LB, Henkel CK (1991) Dendritic and axonal morphology of HRP-injected neurons in the inferior colliculus of the cat. J Comp Neurol 303:75–100

Paxinos G, Watson C (1998) The rat brain, 4th edn. Academic Press, New York

Paxinos G, Kus L, Ashwell KWS, Watson C (1998a) Chemoarchitectonic atlas of the rat brainstem. Academic Press, New York

Paxinos G, Kus L, Ashwell KWS, Watson C (1998b) Chemoarchitectonic atlas of the rat forebrain. Academic Press, New York

Polley DB, Read HL, Storace DA, Merzenich MM (2007) Multiparametric auditory receptive field organization across five cortical fields in the albino rat. J Neurophysiol 97:3621–3638

Prieto JJ, Winer JA (1999) Layer VI in cat primary auditory cortex: Golgi study and sublaminar origins of projection neurons. J Comp Neurol 404:332–358

Rietzel HJ, Friauf E (1998) Neuron types in the rat lateral superior olive and developmental changes in the complexity of their dendritic arbors. J Comp Neurol 390:20–40

Riquelme R, Saldana E, Osen KK, Ottersen OP, Merchan MA (2001) Colocalization of GABA and glycine in the ventral nucleus of the lateral lemniscus in rat: an in situ hybridization and semiquantitative immunocytochemical study. J Comp Neurol 432:409–424

Saldaña E, Aparicio MA, Fuentes-Santamaría V, Berrebi AS (2009) Connections of the superior paraolivary nucleus of the rat: projections to the inferior colliculus. Neuroscience 163:372–387

Sanes DH, Friauf E (2000) Development and influence of inhibition in the lateral superior olivary nucleus. Hear Res 147:46–58

Schneggenburger R, Forsythe ID (2006) The calyx of Held. Cell Tissue Res 326:311–337

Smith PH, Joris PX, Yin TC (1998) Anatomy and physiology of principal cells of the medial nucleus of the trapezoid body (MNTB) of the cat. J Neurophysiol 79:3127–3142

Soares JG, Rosado De Castro PH, Fiorani M, Nascimento-Silva S, Gattass R (2008) Distribution of neurofilament proteins in the lateral geniculate nucleus, primary visual cortex, and area MT of adult Cebus monkeys. J Comp Neurol 508:605–614

Sommer I, Lingenhöhl K, Friauf E (1993) Principal cells of the rat medial nucleus of the trapezoid body: an intracellular in vivo study of their physiology and morphology. Exp Brain Res 95:223–239

Sternberger LA, Sternberger NH (1983) Monoclonal antibodies distinguish phosphorylated and nonphosphorylated forms of neurofilaments in situ. Proc Natl Acad Sci USA 80:6126–6130

Taschenberger H, von Gersdorff H (2000) Fine-tuning an auditory synapse for speed and fidelity: developmental changes in presynaptic waveform, EPSC kinetics, and synaptic plasticity. J Neurosci 20:9162–9173

Trapp BD, Peterson J, Ransohoff RM, Rudick R, Mörk S, Bö L (1998) Axonal transection in the lesions of multiple sclerosis. New Engl J Med 338:278–285

Tsang YM, Chiong F, Kuznetsov D, Kasarskis E, Geula C (2000) Motor neurons are rich in non-phosphorylated neurofilaments: crossspecies comparison and alterations in ALS. Brain Res 861:45–58

Ueyama T, Sato K, Kakimoto S, Houtani T, Sakuma S, Ohishi H, Kase M, Sugimoto T (1999) Comparative distribution of GABAergic and peptide-containing neurons in the lateral lemniscal nuclei of the rat. Brain Res 849:220–225

Van De Werd HJ, Uylings HB (2008) The rat orbital and agranular insular prefrontal cortical areas: a cytoarchitectonic and chemoarchitectonic study. Brain Struct Funct 212:387–401

Van der Gucht E, Vandesande F, Arckens L (2001) Neurofilament protein: a selective marker for the architectonic parcellation of the visual cortex in adult cat brain. J Comp Neurol 441:345–368

Veeranna, Yang DS, Lee JH, Vinod KY, Stavrides P, Amin ND, Pant HC, Nixon RA (2009) Declining phosphatases underlie aging-related hyperphosphorylation of neurofilaments. Neurobiol Aging. doi:10.1016/j.neurobiolaging.2009.12.001

Vickers JC, Costa M (1992) The neurofilament triplet is present in distinct subpopulations of neurons in the central nervous system of the guinea-pig. Neuroscience 49:73–100

Vickers JC, Delacourte A, Morrison JH (1992) Progressive transformation of the cytoskeleton associated with normal aging and Alzheimer's disease. Brain Res 594:273–278

Voelker CC, Garin N, Taylor JS, Gähwiler BH, Hornung JP, Molnár Z (2004) Selective neurofilament (SMI-32, FNP-7 and N200) expression in subpopulations of layer V pyramidal neurons in vivo and in vitro. Cereb Cortex 14:1276–1286

Von Gersdorff H, Borst JG (2002) Short-term plasticity at the calyx of held. Nat Rev Neurosci 3:53–64

West MJ, Slomianka L, Gundersen HJ (1991) Unbiased stereological estimation of the total number of neurons in the subdivisions of the rat hippocampus using the optical fractionator. Anat Rec 231:482–497

Winer JA, Larue DT (1996) Evolution of GABAergic circuitry in the mammalian medial geniculate body. Proc Natl Acad Sci USA 93:3083–3087

Winer JA, Prieto JJ (2001) Layer V in cat primary auditory cortex (AI): cellular architecture and identification of projection neurons. J Comp Neurol 434:379–412

Winer JA, Kelly JB, Larue DT (1999) Neural architecture of the rat medial geniculate body. Hear Res 130:19–41

Wong P, Kaas JH (2008) Architectonic subdivisions of neocortex in the gray squirrel (*Sciurus carolinensis*). Anat Rec (Hoboken) 291:1301–1333

Wong P, Kaas JH (2009) Architectonic subdivisions of neocortex in the tree shrew (*Tupaia belangeri*). Anat Rec (Hoboken) 292:994–1027

Wu SH, Kelly JB (1991) Physiological properties of neurons in the mouse superior olive: membrane characteristics and postsynaptic responses studied in vitro. J Neurophysiol 65:230–246

Wu SH, Kelly JB (1993) Response of neurons in the lateral superior olive and medial nucleus of the trapezoid body to repetitive stimulation: intracellular and extracellular recordings from mouse brain slice. Hear Res 68:189–201

Wu SH, Kelly JB (1995) Inhibition in the superior olivary complex: pharmacological evidence from mouse brain slice. J Neurophysiol 73:256–269

Zhang DX, Li L, Kelly JB, Wu SH (1998) GABAergic projections from the lateral lemniscus to the inferior colliculus of the rat. Hear Res 117:1–12

Zilles K (1985) The cortex of the rat. A stereotaxic atlas. Springer, Berlin